IEEE Access
Multidisciplinary ⋮ Rapid Review ⋮ Open Access Journal

Received November 13, 2018, accepted December 3, 2018, date of publication December 18, 2018, date of current version February 8, 2019.

Digital Object Identifier 10.1109/ACCESS.2018.2888499

Image Denoising Based on HOSVD With Iterative-Based Adaptive Hard Threshold Coefficient Shrinkage

SHANSHAN GAO[1,2], NINGNING GUO[1,2], MINGLI ZHANG[3], JING CHI[1,2], AND CAIMING ZHANG[1,4]

[1]School of Computer Science and Technology, Shandong University of Finance and Economics, Jinan 250014, China
[2]Shandong China-U.S. Digital Media International Cooperation Research Center, Jinan 250014, China
[3]Montreal Neurological Institute, McGill University, Montreal, QC H3A 0E7, Canada
[4]Shandong Co-Innovation Center of Future Intelligent Computing, Yantai 264025, China

Corresponding author: Shanshan Gao (gsszxy@aliyun.com)

This work was supported in part by the Natural Science Foundation of China under Grant 61772309 and Grant 61572286, in part by the NSFC Joint Fund with Zhejiang under Key Project under Grant U1609218, in part by the Key Research and Development Project of Shandong Province under Grant 2017GGX10109 and Grant 2016GSF120013, in part by the Shandong Natural Science Foundation through the Joint Fund for Excellent Young Talents of Provincial Universities under Grant ZR201709190125, and in part by the Fostering Project of Dominant Discipline and Talent Team of Shandong Province Higher Education Institutions.

ABSTRACT Natural images often have self-similarity, which can be used to remove noise. Therefore, many current denoising methods denoise by processing similar image block matrix. Aiming at the problem that these methods will destroy the two-dimensional structure of image blocks when they are expanded into one-dimensional column vectors, a new image denoising method based on high-order singular value decomposition is proposed. Several similar image blocks are stacked into three-dimensional arrays and treated as a third-order tensor; then, higher-order singular value decomposition can be performed. For the core tensor obtained by decomposition, an iterative algorithm with adaptive hard threshold coefficient shrinkage is proposed. The experimental results show that the proposed method outperforms the state-of-the-art methods in peak-signal-to-noise ratio, structural similarity, and visual effects.

INDEX TERMS Image denoising, tensor, high order singular value decomposition, adaptive hard thresholding, threshold coefficient shrinkage.

I. INTRODUCTION

Image denoising is a fundamental problem in image processing. In the process of acquisition and transmission, the image is often affected by the factors of the image device itself and the external environmental conditions, which inevitably generates noise points. The denoising of the image not only provides an image with good visual quality, but also provides a good basis for later image analysis and understanding.

For a noise image $Y = X + D$, where X is the original image and D is Gaussian noise, $D \sim N(0, \sigma^2)$. The task is to obtain a denoised image $\hat{X}$ by processing and calculating the noisy image Y, and make the error between denoised image $\hat{X}$ and original image X is the smallest.

Classic image denoising methods can be divided into spatial domain and frequency domain methods. Traditional spatial domain linear filtering includes mean filtering, median filtering, Wiener [1] filtering, etc. Frequency domain denoising methods include wavelet denoising [2] and partial differential equation denoising [3] and sparse transformation [4] denoising method, etc. Among them, more and more attention has been paid to the transform domain denoising method, and a lot of meaningful discussions and practices have been carried out. It assumes that the real image signal can be approximated by a linear combination of a set of bases, that is to say, the real image signal can be represented in the transform domain sparsely. Due to the advantages of sparse coding in image information representation, it is widely used in the field of image denoising. Reference [5] is a method of wavelet threshold shrinkage, it can achieve denosing based on the assumption that the expression coefficients obtained by wavelet basis transform satisfy the sparsity. In order to achieve translation invariance, Pennec and Mallat [6] proposed to replace the compact expression with redundant expression. However, the above method of sparse

2169-3536 (c) 2018 IEEE. Translations and content mining are permitted for academic research only. Personal use is also permitted, but republication/redistribution requires IEEE permission. See http://www.ieee.org/publications_standards/publications/rights/index.html for more information.

and redundant representation of transform domain adopts data-independent basis, and does not consider the characteristics of the image itself in image denoising application. Yang *et al.* [7] proposed a sparse and redundant expression K-SVD based on dictionary training. The method obtained an overcomplete dictionary by learning, and considers that each image block could be approximated by a linear combination of dictionary atoms, and the coefficient vector had sparsity, that is, most elements in the vector were zero. In recent years, the weighted nuclear norm minimization (WNNM) [8] and the bidirectional low rank representation denoising method based on adaptive cluster dictionary [9] decompose the image into singular values in the transform domain, and perform singular value threshold shrinkage to achieve image denoising. These two methods are still essentially denoising methods based on sparse transforms.

In 2005, Buades *et al.* [10] proposed the concept of non-local similarity of images, and proposed NLM (Non-Local Means) image denoising method, which opened up a new era of image denoising. A partial block has many similar blocks in the entire image. The non-local self-similar prior (NSS) takes advantage of this feature to denoise the image which is the most successful prior to image restoration. Zoran and Weiss proposed an Expected Patch Log Likelihood (EPL) image restoration framework based on image block priors [11], and the prior of image block was modeled by using the Guassian Mixture Model (GMM). This method not only preserved the texture details of the image, but also solved the problem of artificial traces. PGPD [12] put forward a well-defined NSS model learning from natural images, and applies the priori model for high performance denoising, which achieved good denoising effect. However, when used the denoised image block reconstructing the entire image, the image blocks overlap each other in order to overcome the block effect at the edge of the image block. Therefore, one pixel point in the image corresponds to multiple denoising estimates. Inspired by non-local average self-similarity and sparse coding, Mairal *et al.* [13] proposed a Learned Simultaneous Sparse Coding (LSSC) method which was considered that the coding of each image block was not independent of each other and the coding similarity of the image block should be enhanced. Dong *et al.* [4] integrated NSS and local sparse coding into NCSR framework, which had powerful image restoration capability. Dabov *et al.* [14] combined the non-local similarity of image and transform domain denoising method, and proposed BM3D (Block Matching 3-D) image denoising algorithm, which is one of the most classical denoising algorithms. Rajwade *et al.* [15] performed high-order Singular Value Decomposition (HOSVD) on the 3D similar block array in BM3D algorithm, and obtained the dynamic adaptive basis of 3D transform, and excellent denoising effect has also been achieved. The basis of this article is the two algorithms.

The rest of the paper is organized as follows: Part 2 briefly introduces the related work of 3D similar block transform denoising; combined with the properties of high-order singular value decomposition of tensor, Part 3 proposes the new HOSVD denoising algorithm based on iterative-based adaptive hard threshold coefficient shrinkage; the experimental results in Part 4 show the effectiveness of our proposed algorithm; the final part summarizes the full text and proposes the next step.

II. RELATED WORK

At present, the majority of image denoising algorithms utilize the non-local similarity of image blocks. However, when processing image blocks, most of the algorithms expand them into column vectors, which, although it is convenient for calculation and processing, it destroys the 2-dimensional structure information of the image blocks. The two image denoising methods described below still treat the image block as a 2-dimensional matrix structure.

A. BM3D

The BM3D image denoising algorithm is considered to be one of the most classic image denoising algorithms, which combines the non-local similarity of pixel blocks in the image and the denoising of transform domain. The algorithm mainly consists of two stages: basic estimation and final estimation.

1) BASIC ESTIMATION STAGE

For any reference image block $P \in R^{b\times b}$ on the noise image Y, where b is the side length of the reference image block. When perform similar block matching on the noise image Y, denote $S = i : d(P, P_i) \leq T$, $d(P, P_i)$ represents the distance between two image blocks, and T is the threshold of the similarity measure. Then, all of the image blocks $\{P_i\}_{i\in S}$ which satisfy the conditions stacked together to form a 3-dimensional array Z. Perform a 3-dimensional transformation T_{3D} on the 3-dimensional array Z, and then we have a hard threshold shrinkage of the coefficients in the transformation domain, and then carry out 3-dimensional inverse transformation T_{3D}^{-1} to obtain a basic estimation $\hat{Z}$ of Z. As follows:

$$\hat{Z} = T_{3D}^{-1}(H(T_{3D}(Z))) \tag{1}$$

The 3-dimensional transform T_{3D} is composed of 2D-DCT or 2D-Bior1.5 and transform 1D-Haar. H is a hard threshold function. Finally, each image block in $\hat{Z}$ is replaced back to the original position in the image, and a weighted average of each overlapping pixel point results in the basic estimated image Y_{basic}.

2) THE FINAL ESTIMATION STAGE

In the final estimation stage, we can take the basic estimated image Y_{basic} which is obtained in the first stage as a reference. First of all, similar to the first stage, for each reference block P_{basic} on the image Y_{basic}, similar block matching is performed to obtain a 3-dimensional array Z_{basic}. On the noise image, pixel blocks of the same position are selected to form a 3-dimensional Z_{noise}. For the coefficient $c_{basic} \in T_{3D}(Z_{basic})$ of the 3-dimensional transform, select $c_{noise} \in T_{3D}(Z_{noise})$

of the corresponding position, and Eq.(2) can be obtained by Wiener filtering:

$$\hat{c}_{noise} = \frac{c_{basic}^2}{c_{basic}^2 + \sigma^2} c_{noise} \tag{2}$$

The Wiener filter coefficient $\hat{c}_{noise}$ is subjected to 3D inverse transformation to obtain a 3-dimensional array Z_{final}, and then it will be weighted aggregated to the original position on the image, so we can get the final estimate of image denoising Y_{final}.

B. HIGH ORDER SINGULAR VALUE DECOMPOSITION

In recent years, theories about tensor decomposition is optimizing day by day, and their applications are also more and more widely in practice [16], [17]. In [17], the singular value decomposition (SVD) of matrix is extended to tensors, and a high-order SVD method for tensors is proposed. The high-order SVD method has been applied in many fields, such as handwritten numeral recognition [18] and texture analysis [19], and achieved many good results.

Rajwade *et al.* [15] used HOSVD to process the 3-dimensional array in order to achieve image denoising. That is to say, the fixed base of 3D transform in BM3D algorithm is expanded to a dynamic adaptive base and a good denoising effect is achieved.

III. AN ITERATIVE ADAPTIVE HARD THRESHOLD COEFFICIENT SHRINKAGE ALGORITHM

Although the HOSVD image denoising method extends the fixed base in the BM3D method to a dynamic adaptive base, the BM3D algorithm flow is still used, that is to say, the first estimated image obtained by the hard-threshold shrinkage is used as the reference image of the second-stage Wiener filter, and the advantages of HOSVD decomposition and dynamic basis are not fully utilized. The image denoising effect is also slightly inferior to BM3D.

Combining with the properties of high-order singular value decomposition and referring to the processing framework of other image denoising methods [20], [21], an iterative adaptive hard-threshold algorithm is proposed in this paper.

A. SIMILAR BLOCK MATCHING AND HIGH-ORDER SINGULAR VALUE DECOMPOSITION

For each reference block $P^{ref} \in R^{b \times b}$ in the noise image Y, search for K similar blocks (including the reference block itself) P_i, $i = 1, 2, \ldots, K$ which are most similar in image Y. Among them, the similarity measure uses a simple and convenient L_2 distance, which are defined as below:

$$d(P^{ref}, P_i) = \|P^{ref} - P_i\|_2^2 \tag{3}$$

In order to improve the numerical stability of decomposition, the blocks are normalized to each similar block before decomposition [22], [23]:

$$Q_i = P_i - \sum_{i=1}^{K} P_i/K = P_i - \bar{P}, \quad i = 1, 2, \ldots, K \tag{4}$$

To stack all Q_i into 3-dimensional array Z_Q, calculate its high order singular value decomposition,

$$(S_Q, U_1, U_2, U_3) = HOSVD(Z_Q), \tag{5}$$

where S_Q is the core tensor obtained by decomposition, the size is the same as Z_Q which is $b \times b \times K$. U_1, U_2 and U_3 are orthogonal matrices, and the core tensor S_Q can be regarded as the coefficient of the 3-dimensional array Z_Q in the decomposition domain of the high order singular value.

B. ADAPTIVE HARD THRESHOLD COEFFICIENTS SHRINKAGE

How to shrink the coefficient of the core tensor S_Q is the key of denoising algorithm. Based on the assumption that the wavelet coefficients obey the Laplace distribution, [23] and [24] propose a classical threshold function:

$$\tau = \frac{2\sqrt{2}\sigma_w^2}{\sigma_x}, \tag{6}$$

where σ_ω is the estimate of the noise level of the image at the kth iteration of $Y^{(k)}$.

$$\sigma_w = \gamma\sqrt{\sigma^2 - \|Y - Y^{(k)}\|_2^2}, \tag{7}$$

where γ is a preset parameter used to estimate the noise level, and σ_x is the standard deviation of the coefficients of the real image signal X in higher order singular values. Here, notice the properties of the high order singular value decomposition [16], [17]. The core tensor S_Q is a third-order tensor of $b \times b \times K$ size. If slicing in the direction of the vertical third dimension (similar to other dimensions), K different matrix S_Q^i of size $b \times b$ can be obtained.

$$\|S_Q^i\|_F = \sigma_i^{(3)} \quad i = 1, 2, \ldots, K, \tag{8}$$

where $\sigma_i^{(3)}$ is the ith singular value of the third dimension matrix $S_{Q(3)}$ of the core tensor S_Q. Equation (8) can also be expressed as:

$$\sum_{\lambda \in S_Q^i} \lambda^2 = (\sigma_i^{(3)})^2 \quad i = 1, 2, \ldots, K \tag{9}$$

From the formula (8), we can see that the coefficient in the core tensor S_Q is actually to re-decompose the corresponding singular value so that the noise energy originally concentrated on the singular value is mainly transferred to the smaller coefficient in the core tensor S_Q while larger coefficients are less affected by noise. Therefore, this paper adopts the method of hard threshold shrinkage:

$$\hat{S}_Q = hard(S_Q, \tau) \tag{10}$$

In Eq. (6), σ_x is the standard deviation of the coefficients of the real image signal X in higher order singular values

$$\sigma_x = \sqrt{max(\sigma_{S_Q}^2 - \sigma^2, 0)}, \tag{11}$$

where σ_{S_Q} is the standard deviation of the core tensor coefficient S_Q. Since the core tensor S_Q coefficient approximates

This article has been accepted for publication in a future issue of this journal, but has not been fully edited. Content may change prior to final publication. Citation information: DOI 10.1109/ACCESS.2018.2888499, IEEE Access

TABLE 1. Comparison I of different denoising algorithms.

Images	10			20			30		
	BM3D	HOSVD	Ours	BM3D	HOSVD	Ours	BM3D	HOSVD	Ours
C. Man	34.12 0.9304	33.81 0.9242	34.29 0.9311	30.43 0.8730	30.22 0.8611	30.51 0.8729	28.64 0.8360	28.30 0.8081	28.67 0.8 330
Monarc h	34.17 0.9567	34.53 0.9557	34.90 0.9578	30.39 0.9207	30.60 0.9131	31.01 0.9222	28.38 0.8873	28.37 0.8692	28.80 0.8856
Boat	34.31 0.9406	34.31 0.9384	34.51 0.9408	30.54 0.8780	30.56 0.8728	30.73 0.8809	28.55 0.8289	28,48 0.8153	28.68 0.8308
Hill	33.03 0.8972	32.98 0.8971	33.16 0.9004	29.78 0.8138	29.77 0.8143	29.87 0.8166	28.09 0.7548	27.95 0.7477	28.10 0.7537
House	36.73 0.9199	36.77 0.9226	36.78 0.9197	33.85 0.8707	33.40 0.8637	33.92 0.8716	32.23 0.8471	31.25 0.8187	32.24 0.8429
Kod	33.99 0.9360	33.96 0.9322	34.27 0.9356	30.32 0.8784	30.29 0.8715	30.47 0.8783	28.40 0.8348	28.29 0.8195	28.49 0.8321
Lake	32.50 0.9295	32.39 0.9269	32.72 0.9309	28.64 0.8691	28.59 0.8615	28.83 0.8715	26.60 0.8167	26.60 0.8040	26.83 0.8196
Lena	34.81 0.9392	34.70 0.9365	34.89 0.9380	31.13 0.8902	30.92 0.8793	31.15 0.8881	29.13 0.8468	28.80 0.8231	29.06 0.8409
Peppers	35.22 0.9410	35.13 0.9377	35.27 0.9394	31.69 0.9033	31.43 0.8888	31.65 0.8986	29.60 0.8687	29.18 0.8408	29.48 0.8592
Straw	30.95 0.9592	31.21 0.9611	31.50 0.9639	27.13 0.8997	27.23 0.9023	27.37 0.9049	25.01 0.8319	25.07 0.8385	25.14 0.8379
Average	33.98 0.9350	33.97 0.9332	**34.23** **0.9358**	30.39 0.8797	30.30 0.8728	**30.55** **0.8806**	28.46 **0.8353**	28.23 0.8185	**28.55** **0.8336**

the Laplace distribution (see Fig. 1), the average value of the core tensor S_Q coefficients is close to 0 and the variance is

$$\sigma_{S_Q}^2 = \frac{\sum_{i=1}^{m} \lambda_i^2}{m} = \bar{\lambda^2}, \tag{12}$$

where $m(m = b \times b \times K)$ is the number of all the coefficients in the core tensor S_Q and $\lambda_i \in S_Q$ is the coefficient of the core tensor S_Q. Combining the above two equations (9) and (10), we get

$$\sigma_x = \sqrt{max(\bar{\lambda^2} - \sigma^2, 0)} \tag{13}$$

In order to obtain different hard-threshold shrinkage thresholds for each coefficient λ_i, here we propose an adaptive threshold setting method. In the above equation, replace λ_i^2 with $\bar{\lambda^2}$.

$$\sigma_x^i = \sqrt{max(\lambda_i^2 - \sigma^2, 0)} \tag{14}$$

This results in different shrink thresholds for each of the coefficients so that λ_i, which is more heavily affected by noise and smaller, is more shrunk to zero.

In conclusion, the shrinking formula of adaptive hard threshold coefficient proposed in this paper is as follows:

$$\hat{S}_Q = hard(S_Q, \tau_i) \tag{15}$$

$$\tau_i = \frac{2\sqrt{2}\sigma_w^2}{\sigma_x^i}, \tag{16}$$

where σ_w and σ_x^i are determined by formula (6) and (14) respectively.

C. WEIGHTED AGGREGATION AND ITERATIVE REGULARIZATION

After obtaining the contracted core tensor coefficient $\hat{S}_Q$, calculate

$$\hat{Z}_Q = \hat{S}_Q \times_1 U_1 \times_2 U_2 \times_3 U_3 \tag{17}$$

Get the estimated $\hat{Q}_i$ and $\hat{P}_i = \hat{Q}_i + \bar{P}, i = 1, 2, \ldots, K$, $\times_i$ is the tensor and matrix multiplication. Put all the $\hat{P}_i$ back to the original position of the image. Because different image similar blocks may overlap each other, so when we gather a set of 3-dimensional array to define a weight

$$w = \begin{cases} 1/m, & r = 0 \\ r/m, & r > 0 \end{cases} \tag{18}$$

This article has been accepted for publication in a future issue of this journal, but has not been fully edited. Content may change prior to final publication. Citation information: DOI 10.1109/ACCESS.2018.2888499, IEEE Access

TABLE 2. Comparison II of different denoising algorithms.

Images	10			20			30		
	EPLL	NCSR	PGPD	EPLL	NCSR	PGPD	EPLL	NCSR	PGPD
C. Man	32.568 0.8931	32.58 0.8868	30.477 0.8401	29.098 0.8067	29.04 0.7961	29.077 0.7972	27.316 0.7395	27.24 0.7323	27.283 0.7338
Monarc h	36.587 0.9556	36.76 0.9568	34.429 0.9319	32.917 0.9252	33.16 0.9324	33.069 0.9216	28.5 0.895	28.46 0.9088	28.49 0.8987
Boat	33.622 0.8845	33.91 0.8883	32.043 0.8489	30.619 0.8227	30.79 0.8198	30.829 0.8205	28.796 0.7703	28.93 0.7715	29.058 0.7742
Hill	33.508 0.8861	33.69 0.8861	31.871 0.8392	30.451 0.7987	30.65 0.8003	20.683 0.8009	28.809 0.7388	28.97 0.7423	29.115 0.7458
House	35.702 0.9022	32.91 0.8883	34.834 0.885	33.03 0.8623	33.87 0.874	33.808 0.8683	31.332 0.8339	32.07 0.8487	32.172 0.8449
Kod	35.411 0.9118	35.70 0.8978	33.732 0.8697	32.191 0.845	32.41 0.8478	32.594 0.8453	30.549 0.8045	30.84 0.8268	31.137 0.8134
Lake	32.788 0.8816	32.94 0.8819	31.06 0.8447	29.871 0.8255	29.88 0.8202	29.911 0.8209	28.164 0.87847	28.15 0.782	28.197 0.8721
Lena	34.854 0.8911	35.94 0.8971	33.451 0.8648	32.169 0.8446	32.88 0.8553	32.401 0.8469	24.854 0.8095	31.24 0.8288	30.854 0.8177
Peppers	34.857 0.8777	35.75 0.8861	33.525 0.852	32.48 0.8413	33.22 0.8604	32.643 0.8399	30.894 0.8125	31.61 0.8439	31.222 0.8176
Straw	30.861 0.958	32.99 0.9611	28.846 0.9312	26.969 0.8964	27.72 0.8668	27.202 0.8966	24.812 0.825	23.07 0.8486	24.865 0.8194
Average	34.08 0.9042	**34.42** 0.9030	32.43 0.8708	**30.98** 0.8468	31.36 0.8473	31.22 0.8458	29.402 0.8013	**29.958** 0.8133	29.239 0.8048

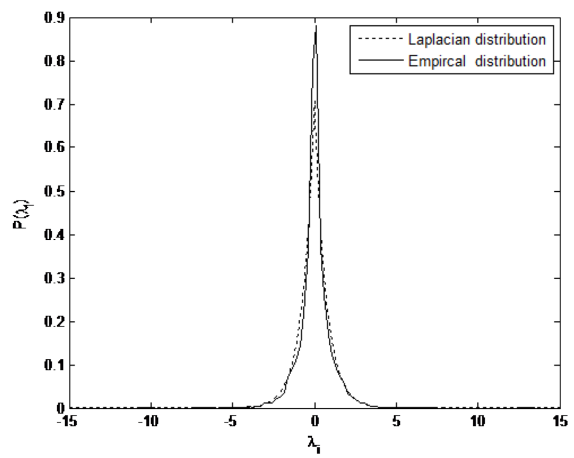

FIGURE 1. The distribution of the core tensor coefficient λ_i of image Peppers.

where r is the number of zero elements in the core tensor of $\hat{S}_Q$, the more zero elements in $\hat{S}_Q$, the greater the weight of the aggregation.

In this way, for the noise image $Y^{(k)}$, we get the estimation $X^{(k)}$ of an iteration. Inspired by [20], [23], and [25], we conduct iterative regularization processing, and update the $Y^{(k+1)}$ at the beginning of the next iteration through the following expression

$$Y^{(k+1)} = (1-\delta)X^{(k)} + \delta Y, \tag{19}$$

where δ is a small positive number that controls the proportion of added noise at each iteration. In summary, the complete algorithm can be described in Algorithm 1.

IV. EXPERIMENTAL RESULTS

In order to verify the correctness of the proposed algorithm, we use 10 standard images of 256×256 size for testing firstly. The experiment parameters are set as follows: the number of iterations $J = 4$, the noise estimation parameter $\gamma = 0.35$ and the iterative regularization parameter $\delta = 0.10$. When the noise level $\sigma \leq 10$, the image side length $b = 6$, $K = 25$, when the noise level is $10 < \sigma \leq 30$, the image side length $b = 7$, $K = 30$. To speed up the algorithm, we take a reference block per 3 pixels, and the search window has a radius of 25 when the similar block matches.

Firstly, we compare our algorithm with the two image denoising algorithms BM3D [14] and HOSVD [15], the basises of the proposed algorithm, which are also based on

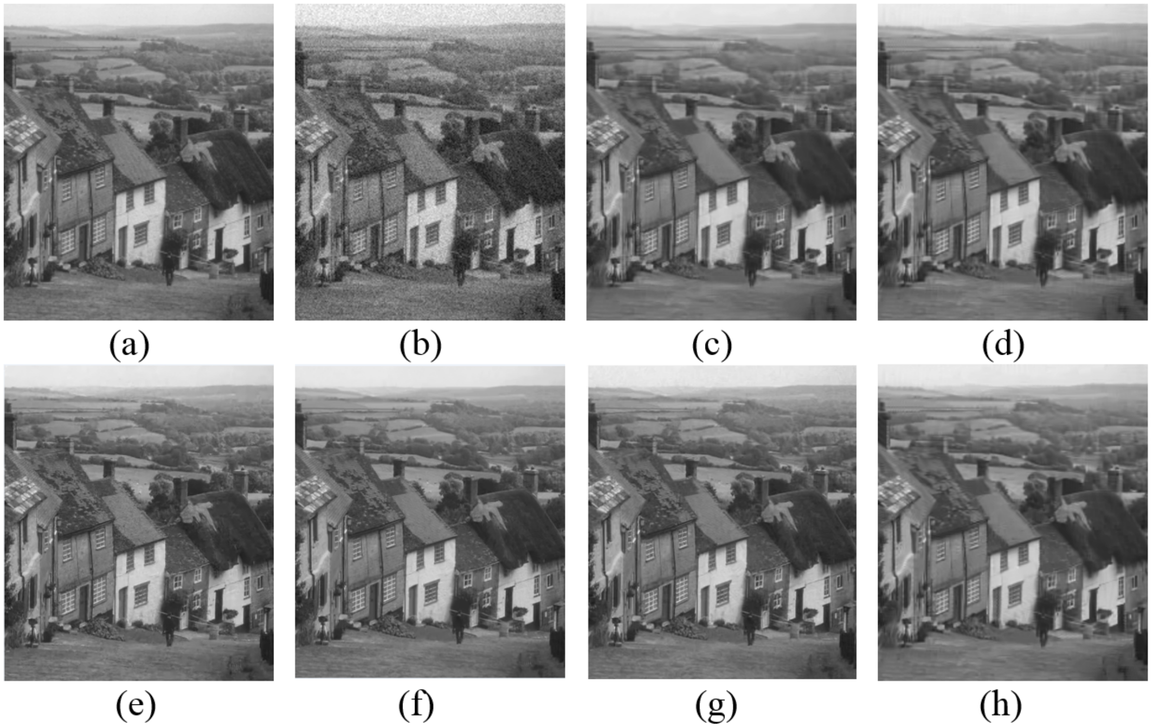

FIGURE 2. Noisy image comparison of image Hill. (a) Initial image, (b) Noise image($\sigma = 10$), (c) BM3D(PSNR=33.03dB, SSIM=0.8972), (d) HOSVD(PSNR=32.98dB, SSIM=0.8971), (e) EPLL(PSNR=33.50758dB, SSIM=0.8861), (f) NCSR(PSNR=33.69dB, SSIM=0.8861), (g) PGPD(PSNR=31.871dB, SSIM=0.8392), (h) Ours(PSNR=33.16dB, SSIM=0.9004).

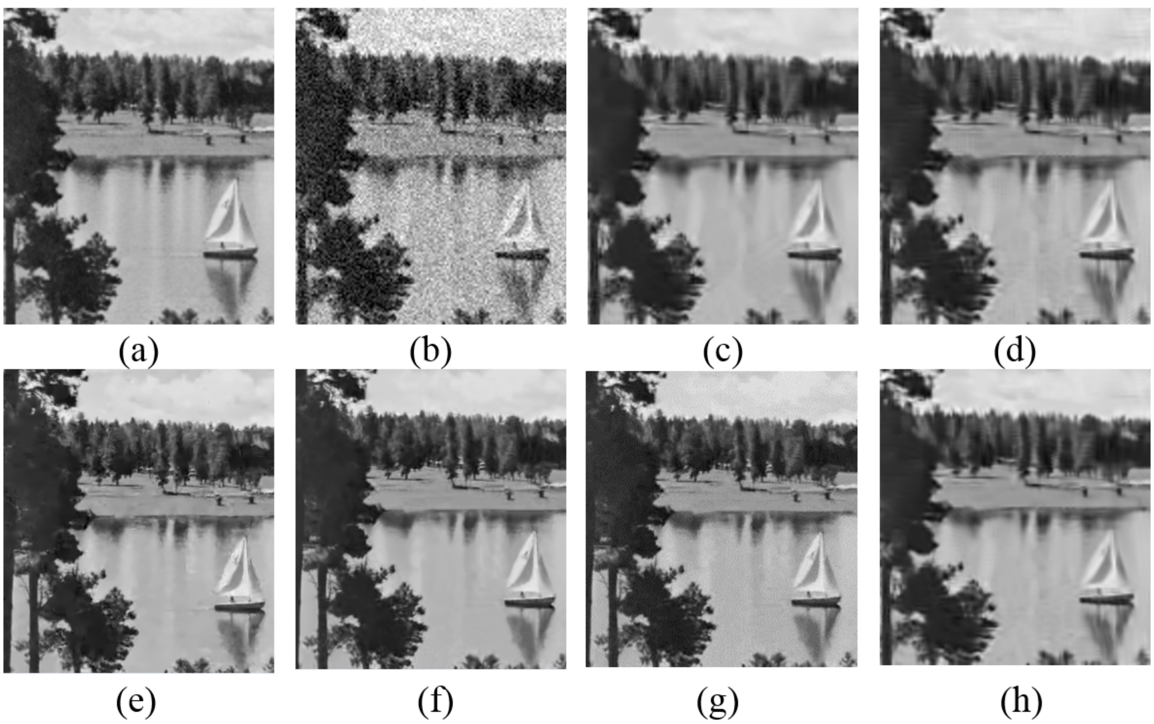

FIGURE 3. Noisy image comparison of image Lake. (a) Initial image, (b) Noise image($\sigma = 20$), (c) BM3D(PSNR=28.64dB, SSIM=0.8691), (d) HOSVD(PSNR=28.59dB, SSIM=0.8615), (e) EPLL(PSNR=29.87111dB, SSIM=0.8255), (f) NCSR(PSNR=29.88dB, SSIM=0.8202), (g) PGPD(PSNR=29.9109dB, SSIM=0.8209), (h) Ours(PSNR=28.83dB, SSIM=0.8715).

3D image block transform. At the same time, in order to verify the algorithms effectiveness, three other related classical algorithms are used for comparison, including EPLL [11], NCSR [4] and PGPD [12]. Peak signal-to-noise ratio (PSNR) and structural similarity (SSIM) are two common image quality metrics. Since the PSNR does not take into account

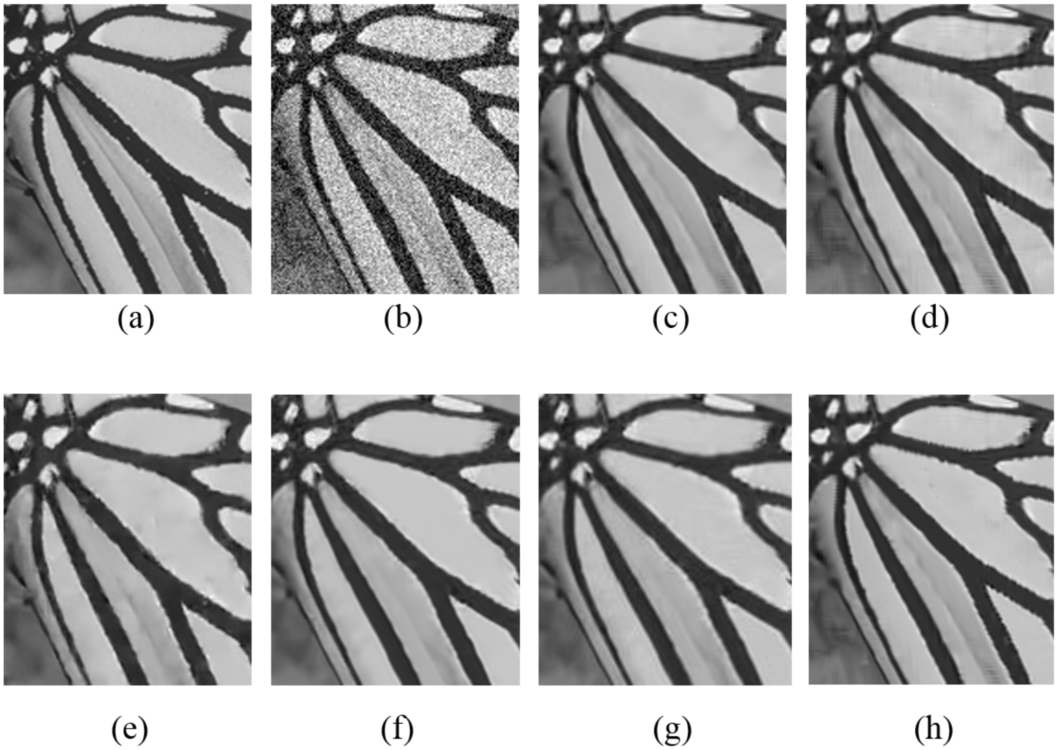

FIGURE 4. Noisy image comparison of image Monarch. (a) Initial image, (b) Noise image(σ = 10), (c)BM3D(PSNR=28.38dB, SSIM=0.8873), (d) HOSVD(PSNR=28.37dB, SSIM=0.8692), (e) EPLL(PSNR=28.5dB, SSIM=0.895), (f) NCSR(PSNR=28.46dB, SSIM=0.9088), (g) PGPD(PSNR=28.49dB, SSIM=0.8209), (h) Ours(PSNR=28.80dB, SSIM=0.8856).

Algorithm 1 Iterative Algorithm Based on HOSVD

Input: Noisy image Y;
Output: Denoising image $X^{(J)}$;
Initialization: $Y^{(l)} = Y$;
Iteration J, $k = 1, 2, \ldots, J$;
Step(1): similar block matching: in image $Y^{(k)}$, find the most similar k image block for each reference block P^{ref};
Step(2): block standardization: use (4) to standardize each set of similar blocks;
Step(3): HOSVD decomposition: $(S_Q, U1, U2, U3) = HOSVD(Z_Q)$;
Step(4): adaptive hard threshold shrinkage: the coefficient shrinkage of S_Q is performed by equation (15);
Step(5): inverse transform to image space, using equation (18) weighted aggregate to get $X^{(k)}$;
Step(6): if k is less than J, use formula (19) to update $Y^{(k+1)}$, and continue to iterate, if k is equal to J, output $X^{(J)}$, the algorithm ends.

the visual characteristics of the human eye, it often occurs that the evaluation result is inconsistent with the subjective feeling of the person. SSIM measures image similarity from the aspects of brightness, contrast and structure, so it is better than PSNR in image denoising and image similarity evaluation. Tables 1 and 2 show the test results of the above six algorithms at 3 different noise levels 10, 20, 30. In each cell of the table, the above values are PSNR values, and the values below are SSIM values. Table 1 and Table 2 show that the new algorithm achieves better PSNR value than the basic two algorithms BM3D and HOSVD algorithms, and is slightly lower than EPLL, NCSR and PGPD in different noise levels. But SSIM is almost higher than all comparison methods.

For a comparison of the visual quality of images after denoising, the reader can see Fig. 2-Fig. 4. It can be seen from the Lake image in Fig. 3 that the forest obtained by the new method is more clear. From the Monarch image in Fig. 4, the new method is better for the texture details of the butterfly wings. Combine PSNR, SSIM value and subjective comparison and we can see that the proposed method can better preserve the details of the image, especially when the noise level is small or the image has more texture details, the denoising effect of the new method is more obvious.

For the above experimental examples, it can be seen that the proposed iterative algorithm has certain advantages for images with a resolution of 256*256, and the running time cost is relatively low. In order to verify the practicability of the algorithm, we have carried out denoising operations on the high-resolution images (with a resolution of 512*512) of

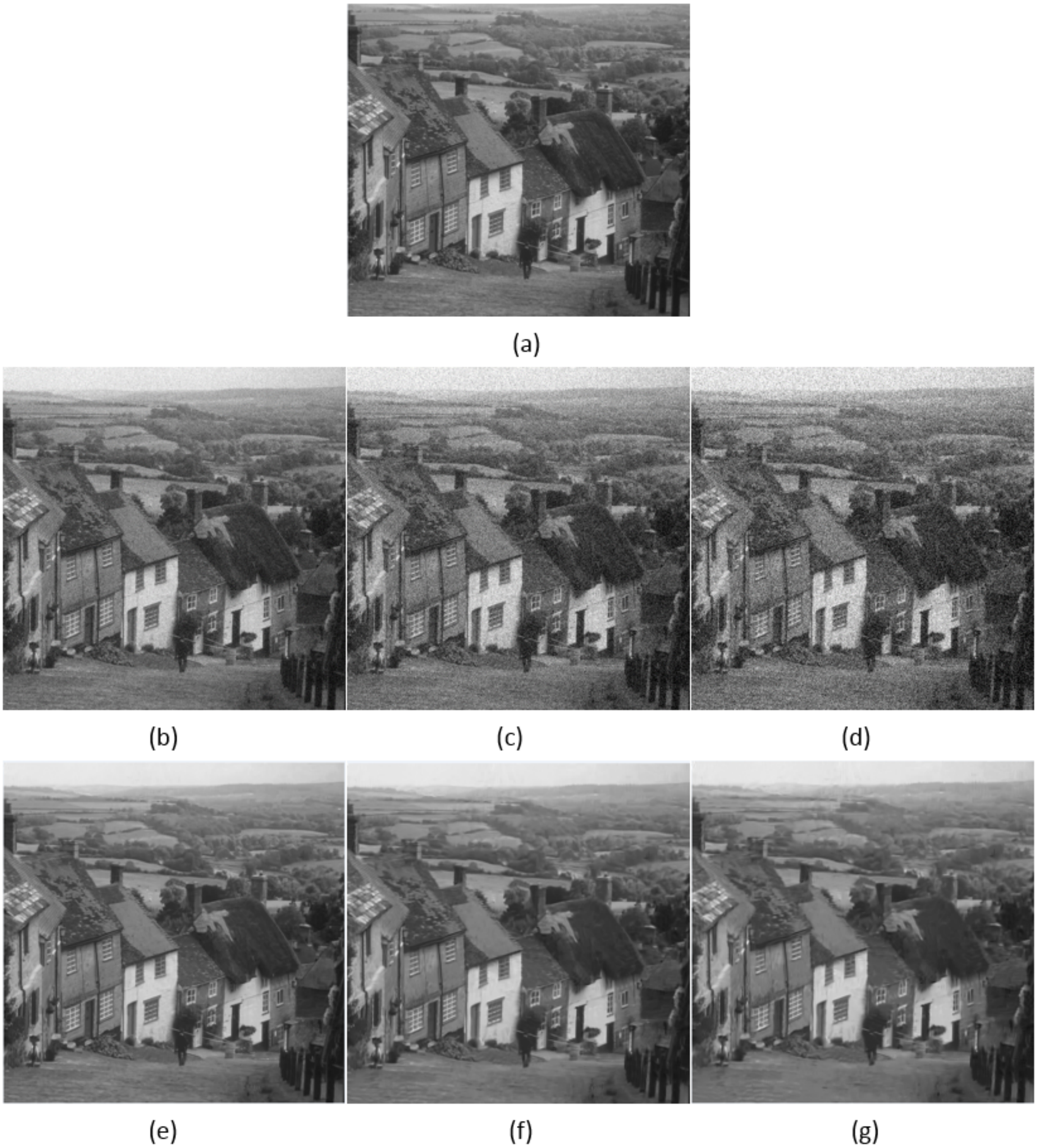

FIGURE 5. Denoising results of high resolution noisy images Hill. (a) Initial image, (b) Noise image($\sigma = 10$), (c) Noise image($\sigma = 20$), (d) Noise image($\sigma = 30$), (e) Denoising result($\sigma = 10$), (f) Denoising result($\sigma = 20$), (g) Denoising result($\sigma = 30$).

the above 10 images. Fig. 5 and Table 3 show the denoising results (Due to layout reason, only image Hill is selected for display). Among them, it can be seen from the visual effect of Fig. 5 that the proposed algorithm can achieve denoising of high-resolution images, and also obtains better results, retaining as much details as possible, such as windows, fences, and lines on the road and so on. Table 3 gives the PSNR and SSIM values for the denoising results of the Hill image at different noise levels. From Table 3, it can be seen that its PSNR and SSIM values are maintained at a high level. The effectiveness and practicability of the algorithm are illustrated. However, for the denoising of high-resolution images, the algorithm also has the same problems as other algorithms, namely, the time cost is greatly improved with the increase of resolution. In the next study, we will try to solve the problem of time cost.

TABLE 3. PSNR and SSIM of denoised image Hill with different σ.

Image	$\sigma = 10$	$\sigma = 20$	$\sigma = 30$
Hill	PSNR: 33.7521 SSIM: 0.8879	PSNR: 30.7924 SSIM: 0.8090	PSNR: 29.1068 SSIM: 0.7499

V. CONCLUSION

In this paper, we propose an iterative algorithm for adaptive hard threshold shrinkage of kernel tensor coefficients.

It is based on the image denoising algorithms BM3D and HOSVD, and is combined with the properties of tensor high order singular value decomposition. The experimental results show that the denoising effect of this algorithm is comparable and outperforms BM3D and HOSVD algorithms to some extent. Under the two measurement standards of PSNR and SSIM, the new algorithm obtains higher measurement values. Compared with other classical algorithms, the proposed algorithm also has obvious advantages in most cases. In terms of visual comparison, it can also maintain better details than other methods after denosing.

If the 3-dimensional array formed by accumulation of similar blocks is regarded as a third order tensor, we can try other forms of tensor decomposition in the next step, such as CP decomposition [26], T-SVD decomposition [27] and so on, exploring appropriate coefficient shrinkage method, so as to achieve better denoising effect.

REFERENCES

[1] N. Wiener, *Extrapolation, Interpolation, and Smoothing of Stationary Time Series, With Engineering Applications*, vol. 113, no. 21. Cambridge, MA, USA: MIT Press, 1964, pp. 1043–1054.

[2] J.-L. Starck, E. J. Candes, and D. L. Donoho, "The curvelet transform for image denoising," *IEEE Trans. Image Process.*, vol. 11, no. 6, pp. 670–684, Jun. 2002.

[3] Y. Xie, S. Gu, Y. Liu, W. Zuo, W. Zhang, and L. Zhang, "Weighted schatten, *p*-norm minimization for image denoising and background subtraction," *IEEE Trans. Image Process.*, vol. 25, no. 10, pp. 4842–4857, Oct. 2016.

[4] W. Dong, L. Zhang, G. Shi, and X. Li, "Nonlocally centralized sparse representation for image restoration," *IEEE Trans. Image Process.*, vol. 22, no. 4, pp. 1620–1630, Apr. 2013.

[5] J. Yang, J. Wright, T. S. Huang, and Y. Ma, "Image super-resolution via sparse representation," *IEEE Trans. Image Process.*, vol. 19, no. 11, pp. 2861–2873, Nov. 2010.

[6] E. L. Pennec and S. G. Mallat, "Geometrical image compression with bandelets," *Proc. SPIE*, vol. 5150, pp. 1273–1286, Jun. 2003.5

[7] J. Yang, J. Wright, T. Huang, and Y. Ma, "Image super-resolution as sparse representation of raw image patches," in *Proc. IEEE Conf. Comput. Vis. Pattern Recognit. (CVPR)*, Jun. 2008, pp. 1–8.

[8] S. Gu, L. Zhang, W. Zuo, and X. Feng, "Weighted nuclear norm minimization with application to image denoising," in *Proc. IEEE Conf. Comput. Vis. Pattern Recognit.*, Jun. 2014, pp. 2862–2869.

[9] X. Li, W. Wang, X. Feng, X. Liu, and L. Luo, "Image denoising via bidirectional low rank representation with cluster adaptive dictionary," *IET Image Process.*, vol. 10, no. 12, pp. 952–961, Dec. 2017.

[10] A. Buades, B. Coll, and J.-M. Morel, "A non-local algorithm for image denoising," in *Proc. IEEE Comput. Soc. Conf. Comput. Vis. Pattern Recognit.*, vol. 2, Jun. 2005, pp. 60–65.

[11] D. Zoran and Y. Weiss, "From learning models of natural image patches to whole image restoration," in *Proc. IEEE Int. Conf. Comput. Vis.*, Nov. 2011, pp. 479–486.

[12] J. Xu, L. Zhang, W. Zuo, D. Zhang, and X. Feng, "Patch group based nonlocal self-similarity prior learning for image denoising," in *Proc. IEEE Int. Conf. Comput. Vis.*, Dec. 2015, pp. 244–252.

[13] J. Mairal, F. Bach, J. Ponce, G. Sapiro, and A. Zisserman, "Non-local sparse models for image restoration," in *Proc. IEEE 12th Int. Conf. Comput. Vis.*, Oct. 2009, pp. 2272–2279.

[14] K. Dabov, A. Foi, V. Katkovnik, and K. Egiazarian, "Image denoising by sparse 3-D transform-domain collaborative filtering," *IEEE Trans. Image Process.*, vol. 16, no. 8, pp. 2080–2095, Aug. 2007.

[15] A. Rajwade, A. Rangarajan, and A. Banerjee, "Image denoising using the higher order singular value decomposition," *IEEE Trans. Pattern Anal. Mach. Intell.*, vol. 35, no. 4, pp. 849–862, Apr. 2013.

[16] T. G. Kolda and B. W. Bader, "Tensor decompositions and applications," *SIAM Rev.*, vol. 51, no. 3, pp. 455–500, 2009.

[17] L. De Lathauwer, B. De Moor, and J. Vandewalle, "A multilinear singular value decomposition," *SIAM J. Matrix Anal. Appl.*, vol. 21, no. 4, pp. 1253–1278, 2000.

[18] B. Savas and L. Eldén, "Handwritten digit classification using higher order singular value decomposition," *Pattern Recognit.*, vol. 40, no. 3, pp. 993–1003, Mar. 2007.

[19] R. Costantini, L. Sbaiz, and S. Susstrunk "Higher order SVD analysis for dynamic texture synthesis," *IEEE Trans. Image Process.*, vol. 17, no. 1, pp. 42–52, Jan. 2008.

[20] W. Dong, G. Shi, and X. Li, "Nonlocal image restoration with bilateral variance estimation: A low-rank approach," *IEEE Trans. Image Process.*, vol. 22, no. 2, pp. 700–711, Feb. 2013.

[21] W. Dong, X. Li, L. Zhang, and G. Shi, "Sparsity-based image denoising via dictionary learning and structural clustering," in *Proc. Comput. Vis. Pattern Recognit. (CVPR)*, Jun. 2011, pp. 457–464.

[22] M. Elad and M. Aharon, "Image denoising via sparse and redundant representations over learned dictionaries," *IEEE Trans. Image Process.*, vol. 15, no. 12, pp. 3736–3745, Dec. 2006.

[23] S. G. Chang, B. Yu, and M. Vetterli, "Adaptive wavelet thresholding for image denoising and compression," *IEEE Trans. Image Process.*, vol. 9, no. 9, pp. 1532–1546, Sep. 2000.

[24] F. Ruggeri and B. Vidakovic, "A Bayesian decision theoretic approach to wavelet thresholding," *J. Amer. Stat. Assoc.*, vol.93, pp.173–179, 1995.

[25] S. Osher, M. Burger, D. Goldfarb, J. Xu, and W. Yin, "An iterative regularization method for total variation-based image restoration," *Multiscale Model. Simul.*, vol. 4, no. 2, pp. 460–489, 2005.

[26] H. A. L. Kiers, "Towards a standardized notation and terminology in multiway analysis," *J. Chemometrics*, vol. 14, no. 3, pp. 105–122, 2000.

[27] M. E. Kilmer and C. D. Martin, "Factorization strategies for third-order tensors," *Linear Algebra Appl.*, vol. 435, no. 3, pp. 641–658, 2011.

SHANSHAN GAO received the B.S. degree from the Shandong University of Technology, Zibo, China, in 2001, and the M.S. and Ph.D. degrees from Shandong University, Jinan, China, in 2005 and 2011, respectively. She is currently a Professor with the School of Computer Science and Technology, Shandong University of Finance and Economics. Her current research interests include computer graphics, image saliency detection, and image segmentation.

NINGNING GUO was born in 1994. She is currently pursuing the master's degree with the Academy of Computer Science and Technology, Shandong University of Finance and Economics. Her main research interests include image processing and machine intelligence.

MINGLI ZHANG received the Ph.D. degree in image processing and machine learning from the École de technologie supérieure, University of Quebec, Montreal, in 2017. She is currently a Post-Doctoral Research Fellow with the Mcgill Centre for Integrative Neuroscience/Ludmer Centre for Neuroinformatics and Mental Health, Montreal Neurological Institute, Mcgill University, involving in brain image analysis. Her research interests include designing and application of high-performance machine learning models to solve problems in the fields of computer vision, biomedical imaging, and natural images.

JING CHI received the Ph.D. degree in computer science from the Shandong University, China, in 2012. She is currently an Associate Professor with the Department of Computer Science and Technology, Shandong University of Finance and Economics. Her research interests include computer facial animation, dynamic modeling, and curve fitting.

CAIMING ZHANG received the B.S. and M.E. degrees in computer science from Shandong University, in 1982 and 1984, respectively, and the Dr.Eng. degree in computer science from the Tokyo Institute of Technology, Japan, in 1994. From 1997 to 2000, he held a visiting position at the University of Kentucky, USA. He is currently a Professor and a Doctoral Supervisor with the School of Computer Science and Technology, Shandong University of Finance and Economics. His research interests include CAGD, CG, information visualization, and medical image processing.